MALARIA

Copyright © 2019 The Authors, some rights reserved; exclusive licensee American Association for the Advancement of Science. No claim to original U.S. Government Works

Identifying purine nucleoside phosphorylase as the target of quinine using cellular thermal shift assay

Jerzy M. Dziekan[1], Han Yu[1], Dan Chen[1], Lingyun Dai[1], Grennady Wirjanata[1], Andreas Larsson[2], Nayana Prabhu[1], Radoslaw M. Sobota[3,4], Zbynek Bozdech[1]*, Pär Nordlund[1,3,2]*

Mechanisms of action (MoAs) have been elusive for most antimalarial drugs in clinical use. Decreasing responsiveness to antimalarial treatments stresses the need for a better resolved understanding of their MoAs and associated resistance mechanisms. In the present work, we implemented the cellular thermal shift assay coupled with mass spectrometry (MS-CETSA) for drug target identification in *Plasmodium falciparum*, the main causative agent of human malaria. We validated the efficacy of this approach for pyrimethamine, a folic acid antagonist, and E64d, a broad-spectrum cysteine proteinase inhibitor. Subsequently, we applied MS-CETSA to quinine and mefloquine, two important antimalarial drugs with poorly characterized MoAs. Combining studies in the *P. falciparum* parasite lysate and intact infected red blood cells, we found *P. falciparum* purine nucleoside phosphorylase (PfPNP) as a common binding target for these two quinoline drugs. Biophysical and structural studies with a recombinant protein further established that both compounds bind within the enzyme's active site. Quinine binds to PfPNP at low nanomolar affinity, suggesting a substantial contribution to its therapeutic effect. Overall, we demonstrated that implementation of MS-CETSA for *P. falciparum* constitutes a promising strategy to elucidate the MoAs of existing and candidate antimalarial drugs.

INTRODUCTION

Malaria is a vector-borne disease caused by five protozoan species of the *Plasmodium* genus prevailing in tropical and subtropical regions. Ongoing efforts to eradicate malaria have reduced considerably its worldwide burden and mortality over the past decade (*1*). However, malaria still remains a substantial health problem with 216 million cases and 445,000 deaths in 2016 alone, as estimated by the World Health Organization (WHO) (*1*). Recent success in malaria control can be attributed to effective vector-control strategies, as well as the mass implementation of artemisinin combination therapies (ACTs). However, an increased mosquito resistance to commonly used insecticides (*2*) and decreased responsiveness of the malaria parasite to the standard ACTs (*3*) threaten major escalation in malaria incidence in the near future. Recent reports of increased failure rates of artesunate-amodiaquine treatment in western Cambodia are particularly worrisome, considering that it is already the fifth ACT failing in that region (*4*). In the past, the emergence of resistance to clinically used antimalarial drugs typically signaled their subsequent failure, eventually rendering them obsolete in all affected areas around the globe (*5*).

The vast majority of clinically used antimalarial drugs were not rationally designed to interfere with a specific molecular target but rather were identified on the basis of their potent antimalarial properties in phenotypic screenings (*6*). Consequently, the understanding of their mechanisms of action (MoAs) remains rudimentary in most cases. Among all available antimalarial drugs, besides artemisinins, quinolines represent the largest and undoubtedly the most clinically important group. From these, quinine, mefloquine, and chloroquine are among the most widely used antimalarial drugs, which remain in clinical use until today (*7*). Although the antimalarial effect of chloroquine appears strongly associated with the inhibition of heme detoxification in the parasite's digestive vacuole (*8*), MoAs of other quinolines remain largely elusive (*9*, *10*). Quinine, first isolated in 1820 from a *Cinchona* tree bark, became the first-in-class quinoline (*7*). Currently, it represents an essential alternative for the treatment of severe malaria and remains the treatment of choice for uncomplicated malaria in pregnant women during the first trimester (*11*). Over the years, a range of its derivatives were synthesized, including mefloquine developed by the Walter Reed Army Institute of Research in 1984 (*12*). Today, mefloquine is a crucial partner drug within the ACT formulations, particularly those used in Southeast Asia, and remains an important chemoprophylaxis agent for malaria (*13*, *14*). Resistance to both drugs was reported in Southeast Asia in the 1980s and was associated with an increased copy number of the *pfmdr1* gene (*15*). *Pfmdr1* encodes a transmembrane transporter PfPGH1 that is believed to mediate drug efflux from the cytoplasm to the digestive vacuole (*16*). This suggests that the molecular target of mefloquine/quinine is present in the cytosol, and thus, the MoA of both drugs is (at least partially) distinct from that of chloroquine. Consistent with this, recent findings suggested that mefloquine inhibits translation through 80*S* ribosome binding, although polypharmacology involving other unidentified target(s) is expected (*17*). No specific targets of quinine have been discovered to date. Together, the wide knowledge gap remaining in our basic understating of the MoAs of common antimalarial drugs substantially hinders implementation of effective countermeasures to clinical drug failure (*18*).

The cellular thermal shift assay (CETSA), originally developed to assist anticancer drug target studies, is the first broadly applicable label-free method to study drug target engagement in intact cells (*19*–*21*). The technique is based on the discovery that heat unfolded proteins precipitate rapidly in cells, allowing melting curves to be measured by monitoring the remaining soluble proteins after a heat challenge. Akin to the classical thermal shift assay using purified

[1]School of Biological Sciences, Nanyang Technological University, 637551, Singapore. [2]Department of Oncology and Pathology, Karolinska Institutet, Stockholm 17177, Sweden. [3]Institute of Molecular and Cell Biology, Functional Proteomics Laboratory, Agency for Science, Technology and Research (A*STAR), 138673, Singapore. [4]Institute of Medical Biology, Agency for Science, Technology and Research (A*STAR), 138648, Singapore.
*Corresponding author. Email: pnordlund@ntu.edu.sg (P.N.); zbozdech@ntu.edu.sg (Z.B.)

Downloaded from http://stm.sciencemag.org/ by guest on February 8, 2019

proteins (*22*), ligand binding typically leads to protein stabilization and a positive shift in melting temperature (T_m). Coupling CETSA with multiplexed quantitative mass spectrometry (MS-CETSA) allows monitoring of the entire proteome simultaneously for changes in the protein thermostability under drug treatment. As a result, proteins interacting with the drug can be identified in MS-CETSA without previous knowledge of the pathways or mechanisms involved. In this work, we developed an efficient protocol for MS-CETSA studies of *Plasmodium falciparum* and applied it for antimalarial drug target identification. Subsequently, we identified *P. falciparum* purine nucleoside phosphorylase (PfPNP) as a protein target of quinine and mefloquine. Using enzymatic and biophysical in vitro assays, we observed a particularly high-affinity interaction of quinine with PfPNP, suggesting its role in the drug's MoA.

RESULTS

Adaptation of CETSA for *P. falciparum*

In this work, we implemented and validated MS-CETSA for identification of direct protein targets of antimalarial drugs in the *P. falciparum* proteome. We used cellular lysates from in vitro blood-stage *P. falciparum* parasites for studies of direct drug–target interactions ("lysate"). In addition, we used intact *P. falciparum*–infected erythrocytes for studies of drug-target engagements and consequent downstream effects within the cellular context ("intact cell"). Because of potential obstructions of the MS analysis caused by the high abundance of hemoglobin and carbonic anhydrase-1 in the red blood cell (RBC) cytoplasm (*23*), for the in-cell settings, we used magnetic enrichment of *P. falciparum*–infected erythrocytes. The resulting enrichment of infected erythrocytes to >75% was suitable for generating MS data from the intact cells, providing a comprehensive representation of the *P. falciparum* proteome (see below). Overall, we adopted two existing variants of CETSA data collection strategies (Fig. 1): (i) the melt curve CETSA approach, in which protein precipitation is monitored at 10 distinct temperatures in the presence or absence of drug; (ii) the isothermal dose-response (ITDR) CETSA, in which protein stabilization is monitored at multiple drug concentrations at a single temperature. Whereas the melt curve CETSA is used to assess the differences in protein thermal denaturation characteristics between drug-treated and vehicle control samples, the ITDR experiments monitor the change in protein stability under thermal denaturation conditions across a drug concentration gradient. Both melt curve and ITDR experiments can be conducted with cell lysates and intact cells obtained from in vitro *P. falciparum* culture. Note that not all thermal stability shifts are a direct result of drug binding, but they can also be caused by indirect "downstream" effects, such as changes in protein stability due to binding of physiological ligands including metabolites, nucleic acids, or other proteins (*19*, *24*). Such shifts could result from the modulation of cell signaling, metabolism, or stress pathways induced by the drug. Cross-referencing of the lysate and in-cell CETSA datasets provides one of the avenues for discerning between direct and indirect drug effects.

To first assess the melting properties of the *P. falciparum* proteome at the trophozoite stage, we subjected nontreated lysate and intact-cell samples to melt curve CETSA analysis, determining proteome-wide protein thermal stability in the 37° to 73°C temperature range (Fig. 2A). Consequently, we calculated the distribution of individual protein melting temperatures (T_m; equivalent to 50% protein denaturation) within each dataset (Fig. 2B). Overall, the melting profiles

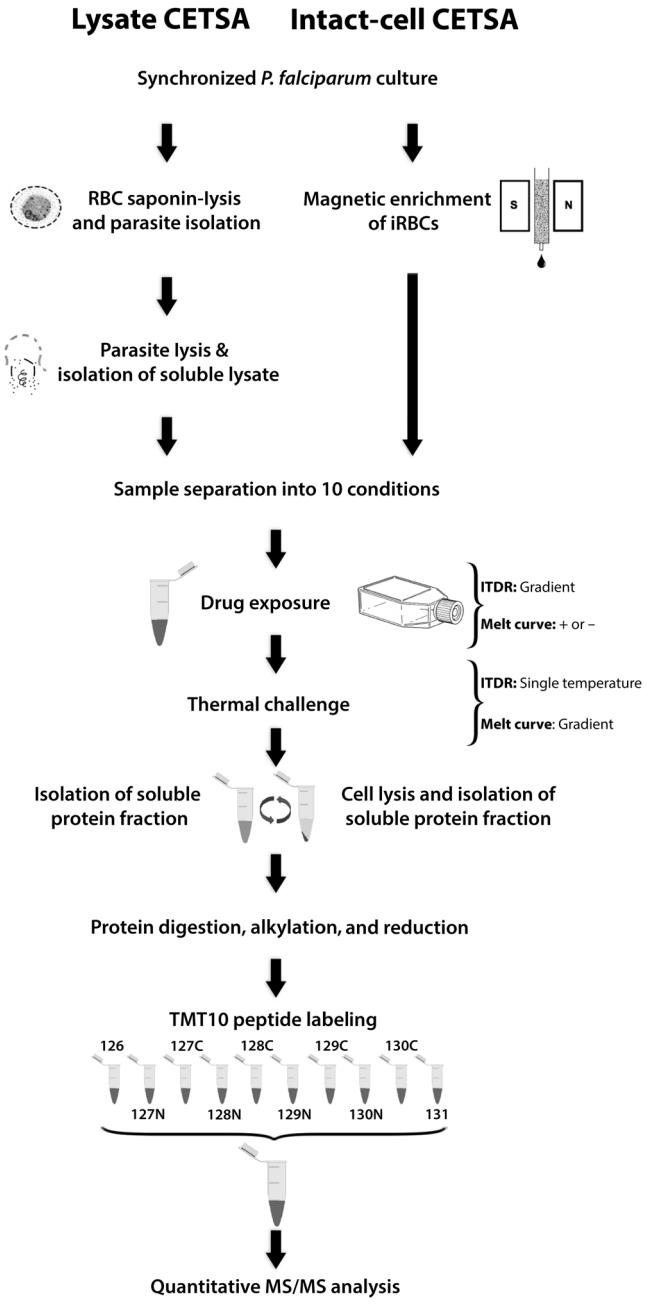

Fig. 1. Schematic illustration of *P. falciparum* CETSA protocol. Lysate and intact-cell CETSA experiments are conducted using soluble parasite protein lysate or magnetic cell sorting–enriched infected RBCs (iRBCs), respectively. In both scenarios, the samples are separated into 10 identical fractions, subjected to drug treatment, and exposed to the thermal challenge to denature and irrevocably precipitate unstable proteins. Two alternative CETSA variants, ITDR or melt curve, can be performed. ITDR involves treating samples with a drug concentration gradient and exposing them to a single temperature, whereas melt curve CETSA relies on the presence or absence of the drug in corresponding samples, which are then heated to 10 distinct temperatures along 37° to 73°C thermal gradient. The soluble protein is isolated by centrifugation and, in case of whole-cell approach, preceded by cell lysis, and samples are reduced, alkylated, digested by lysyl-endopeptidase (Lys-C) and trypsin and then labeled with distinct TMT10 isobaric peptide tags. Peptide abundance across 10 fractions is then quantified through multiplexed MS. After mapping to the plasmodium proteome database, values are translated to protein quantities along the thermal/drug gradient.

Downloaded from http://stm.sciencemag.org/ by guest on February 8, 2019

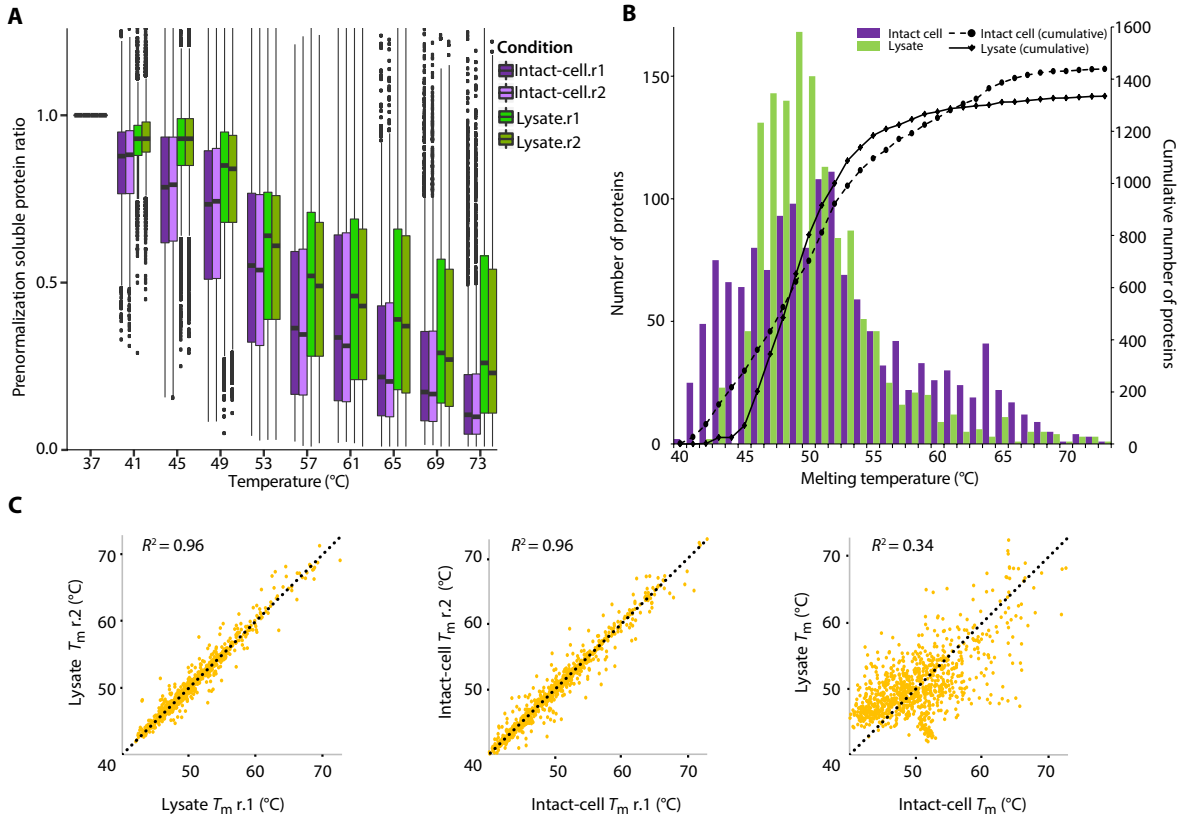

Fig. 2. *P. falciparum* proteome melting behavior. (**A**) Global protein melting behavior in lysate (green) and intact-cell (purple) melt curve CETSA in the absence of drugs. The box plot is drawn on the basis of independent protein melting profiles within each dataset representing remaining soluble protein abundance across the temperature gradient (*x* axis) relative to the nondenaturing 37°C condition (black band) on the *y* axis. Median (second quartile) protein levels are indicated with a black band, first and third quartiles with colored boxes, whereas the lowest/highest datum within 1.5 × IQR (interquartile range) of the lower/higher quartile is represented with whiskers. Data outliers not included within whiskers are plotted as dots. (**B**) Proteome-wide T_m distribution in melt curve CETSA lysate (green) and intact cell (purple). Only proteins achieving >50% denaturation within the thermal gradient, detected at >3 peptide-spectrum matches (PSMs), and with <5°C T_m SD between replicates were included in the analysis. Number of proteins (left, *y* axis) exhibiting T_m at a given temperature (*x* axis) is plotted as bar chart, whereas their cumulative number including proteins with lower T_m is indicated on the right (*y* axis). (**C**) T_m comparison of 964 proteins identified in lysate and intact-cell melt curve. The correlation coefficient (R^2) of linear regression analysis is indicated for each dataset pair. Dashed black trend-line indicates perfect overlap of values in two conditions.

were defined for 2488 proteins in the lysate and 1962 in the intact-cell variant. The proteins isolated from the lysate experiment exhibited apparent higher global thermostability, as demonstrated by the lower degree of denaturation along the entire thermal gradient (Fig. 2A). In particular, there was a substantially higher proportion of thermostable proteins in the lysate (44%), which showed less than 50% decrease in abundance in the soluble fraction after the thermal challenge. These thermostable proteins could represent soluble protein aggregates that are stabilized by the detergent used for host-cell removal before sample generation. Hence, for further analyses, we applied more stringent cutoff criteria to include high-confidence melting profiles, including (i) ≥50% loss in protein abundance at the highest temperature, (ii) T_m within the tested temperature range, and (iii) low variability between replicate measurements (see Materials and Methods). As a result of these stringent criteria, T_m values were determined for 1821 distinct *P. falciparum* proteins in at least one experimental variant, with 1345 of them derived from the lysate and 1439 from the intact-cell condition. On the basis of previously reported proteomics data (*25*), this constitutes 80% of the trophozoite proteome and represents 65% of proteins expressed throughout the entire intraerythrocytic developmental cycle. Analysis of the 946 *P. falciparum* proteins present in both datasets (Fig. 2B) revealed somewhat lower average protein stability in intact cells (ΔT_m = 0.3°C) but distinct melting profiles of the individual proteins in the two conditions (R^2 = 0.34) (Fig. 2C). This is consistent with a similar comparison conducted for human immortalized myelogenous leukemia (K562) cells, which reported lower protein stability in the intact cell, relative to the lysate condition, likely resulting from the crowded environment of the cytoplasm and other intracellular compartments (*21*). We also observed correlated precipitation of many large protein complexes in both melt curve experimental variants (fig. S1), which is in agreement with the concept of thermal proximity coaggregation recently described in human cells (*26*). In addition to the *P. falciparum* proteins, melt curve CETSA in intact cells yielded melting profiles for 362 proteins originating from the host cell. This constitutes the first CETSA data for (a substantial fraction of) the erythrocyte proteome. Here, we found that the global T_m distribution among RBC proteins was, in general, higher than that of the *P. falciparum* or the K562 cell proteome (fig. S2). The T_m analysis of 268 proteins detected in both human proteomes demonstrates differences in protein thermal stability between cell types (R^2 = 0.44), showing that erythrocytic proteins display on average

Downloaded from http://stm.sciencemag.org/ by guest on February 8, 2019

1.7°C higher T_m. The measurement of CETSA data for the erythrocyte proteome can be in principle explored to access interactions and downstream effects with host proteins during antimalarial drug exposure.

CETSA-based methodology for identification of protein drug targets in *P. falciparum*

For the identification of drug-target interactions in *P. falciparum*, we adopted the ITDR variant of the CETSA protocol, using the information gained from the melt curve experiments (Fig. 2). Target protein engagement in ITDR is recognized as protein stabilization in response to increasing drug concentration at a single temperature relative to nondenaturing conditions (see Fig. 1 and Materials and Methods). Data analysis, scaling, and identification of drug-target interactions were carried out using mineCETSA, an in-house–developed R package (see Materials and Methods). First, we carried out an ITDR experiment in lysate with pyrimethamine, the well-characterized antimalarial drug known to inhibit *P. falciparum* dihydrofolate reductase–thymidylate synthase (PfDHFR-TS) (*27*, *28*). Because of the high T_m observed for PfDHFR-TS observed in the CETSA melt curve experiment (fig. S3), the ITDR experiments were carried out at 59° and 65°C. Among 2102 detected proteins, only PfDHFR-TS (PF3D7_0417200) exhibited dose-dependent stabilization by pyrimethamine (Fig. 3A). Protein response was observed at both temperatures, although the stabilization surpassed the "significance threshold for hit selection" only at 65°C (Fig. 3B). The minimal dose threshold (MDT) (i.e., the lowest drug concentration inducing high-confidence protein stabilization) for PfDHFR-TS was ~14.7 nM. This corresponds to the activity concentration range of pyrimethamine previously reported for *P. falciparum* in vitro growth inhibition assays (*29*) and in vitro kinetic studies with purified enzyme (*30*). In addition to ITDR, we also demonstrated the pyrimethamine-dependent stabilization of PfDHFR-TS through the melt curve CETSA assay in lysate (fig. S3).

In the absence of a priori knowledge about the identity of the putative targets of a drug, the thermal challenge temperatures for the ITDR analysis should be selected such that the global proteome is sufficiently sampled. Hence, for the subsequent ITDR analyses, we selected 51°C corresponding to the average T_m for the *P. falciparum* proteome and 57°C to account for the more thermostable portion of the proteome observed in intact-cell samples (Fig. 2B). To validate this strategy in the intact-cell CETSA, we investigated protein target engagement by E64d, a broad-spectrum cysteine protease inhibitor, known to interact with several targets in the *P. falciparum* proteome (*31*–*33*). Accordingly, four proteins exhibited dose-dependent stabilization by E64d in the ITDR (57°C) experiment (Fig. 3, C and D). Three of the stabilized proteins [falcipain 2A (FP2A; PF3D7_1115700), falcipain 3 (FP3; PF3D7_1115400), and dipeptidyl aminopeptidase 1 (DPAP1; PF3D7_1113400)] carry a cysteine protease domain that is expected to be the main target of the drug. In contrast, the fourth identified protein—DSK2 protein homologue (PF3D7_1113400)—does not carry a signature cysteine protease active site in its primary amino acid sequence. The MDTs for all four targets were within low nanomolar range (FP3, ~3 nM; FP2A, ~11 nM; DSK2, ~9 nM; and DPAP1, ~11 nM). Note that this is substantially lower than the micromolar concentrations at which the compound inhibits parasite growth in vitro (*34*). Together, these results demonstrate that CETSA has the capacity to detect direct drug–target binding in the proteome of the malaria parasites with a high degree of specificity.

CESTA-based identification of molecular targets for mefloquine and quinine in *P. falciparum*

Next, we conducted ITDR assays to identify protein targets of quinine and mefloquine. Applying the ITDR (51°C) protocol for lysate samples exposed to quinine (0 to 10 μM) or mefloquine (0 to 100 μM), we identified purine nucleoside phosphorylase (PfPNP; PF3D7_0513300) as the only protein exhibiting high-confidence stabilization among 2157 and 2032 *P. falciparum* proteins detected simultaneously in the two datasets (Fig. 4, A to D). The MDT for PfPNP stabilization was ~0.1 μM for quinine and ~0.6 μM for mefloquine. Crucially, a dose-dependent stabilization of PfPNP was also observed for quinine in the intact-cell ITDR at 57°C with an MDT of ~2.5 nM (Fig. 4, E and F). No stabilization of PfPNP was observed in the two corresponding intact-cell ITDRs conducted with mefloquine, which revealed a dose-dependent stabilization of three other proteins instead (Fig. 4G). Pyruvate kinase II (PfPyKII; PF3D7_1037100) exhibited an early dose-dependent stabilization (MDT, ~19.5 nM) in the intact-cell ITDR (57°C). This was, however, concomitant with an increase of the protein abundance at 37°C, suggesting that the stabilization likely reflects a downstream effect of the drug binding, also leading to increased protein levels (Fig. 4H). Considering PfPyKII is essential for the parasite's metabolism (*35*, *36*), the shift in protein abundance in the reference condition could represent a general stress response to the drug-induced perturbations. The stabilization of the two mitochondrial proteins heat shock protein 70 (Hsp70-3; PF3D7_1134000) and GrpE protein homolog (Mge1; PF3D7_1124700) was also observed in the intact-cell ITDR (57°C) but was detectable only at the highest drug dose (10 μM) (fig. S4). This may reflect an indirect effect on mitochondrial membrane via reactive oxidative species (ROS) induced by mefloquine in the *P. falciparum* cell (*37*). We also detected stabilizations of four ribosomal subunits and a putative subunit of the translation initiation factor 2 by mefloquine in the lysate conditions, albeit the extent of stabilization was considerably lower for each subunit as compared with PfPNP, and they satisfied only two of the three high-confidence cutoff criteria (table S1). This is consistent with previous studies demonstrating mefloquine interaction with the ribosomal complex (*17*). Whereas mefloquine engages a broader spectrum of *P. falciparum* proteins (including PfPNP), in the MS-CETSA, quinine appears to engage PfPNP almost exclusively. This was verified further using Western blotting, directly reproducing the observed change in PfPNP stability (fig. S5). PfPNP has previously been demonstrated to be a promising antimalarial drug target, due to its key function in purine metabolism (*38*, *39*). It is thus conceivable that PfPNP not only plays a major role in the MoA of quinine but could also contribute to that of mefloquine. We also observed stabilization of human mitochondrial 60-kDa heat shock protein (HSPD1; P10809) in response to quinine (MDT, 0.15 μM) in intact-cell ITDR experiments (fig. S6). Currently, little is known about the role of host proteins for parasite growth and/or their roles in drug MoAs; nonetheless, these results may suggest their biological relevance.

In vitro validation of quinine and mefloquine binding with PfPNP

To further assess the interaction of PfPNP with quinine and mefloquine, we investigated binding properties in vitro using heterologously expressed recombinant PfPNP (*40*). First, we monitored the relative stabilizing effect of quinine and mefloquine on PfPNP using differential scanning fluorimetry (DSF) (Fig. 5A). Analogous to CETSA,

Downloaded from http://stm.sciencemag.org/ by guest on February 8, 2019

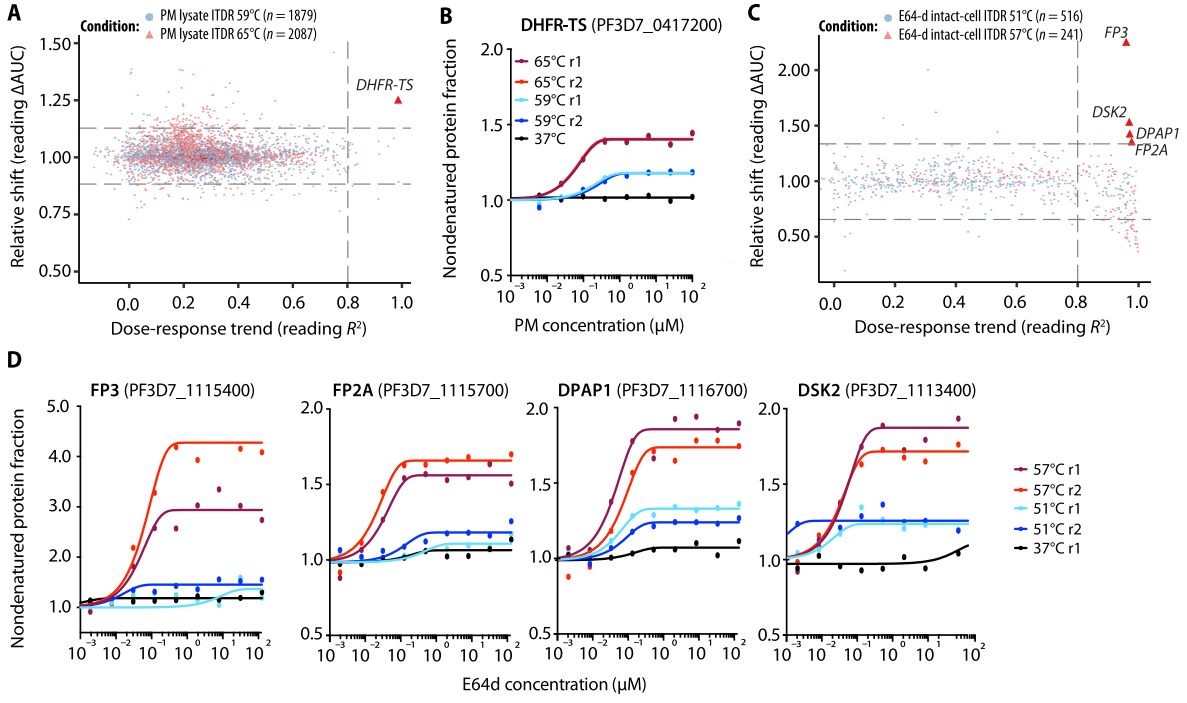

Fig. 3. Protein target engagement by pyrimethamine and E64d. (**A**) Whole proteome analysis in lysate ITDR experiments under 0 to 100 μM pyrimethamine (PM) treatment with thermal challenges at 59°C (blue dots) or 65°C (red triangles). Distribution of protein stabilization is plotted as a function of R^2 value (which quantifies the adherence of protein stabilization profile to the dose-response trend) against ΔAUC (area under the curve of heat-challenged sample normalized against nondenaturing 37°C control) for all proteins detected in the assay and the reference condition ("*n*"). Three times of median absolute deviation (MAD) of ΔAUC in each dataset (MAD × 3) and $R^2 = 0.8$ cutoffs are indicated on the graph. Significant hit – PfDHFR is highlighted in red. (**B**) Protein stabilization curve of PfDHFR identified in (A). The extent of stabilization under thermal denaturation conditions [59°C (blue) or 65°C (red)] is plotted relative to no-drug control with nondenaturing control condition plotted in black. (**C**) Whole proteome analysis in intact-cell ITDR experiments under 0 to 125 μM E64d treatment with thermal challenges at 51°C (blue dots) or 57°C (red triangles). Distribution of protein stabilization is plotted as a function of R^2 value against ΔAUC, similarly as in (A). (**D**) Protein stabilization curves of hits identified in (C). The extent of stabilization under thermal denaturation conditions [51°C (blue) or 57°C (red)] is plotted relative to no-drug control with nondenaturing control condition plotted in black.

DSF assesses ligand-mediated thermal stabilization of a protein by monitoring protein unfolding as indicated by fluoroprobe binding to the protein's hydrophobic regions. The extent of thermal stabilization of recombinant PfPNP was determined for quinine, mefloquine, and other quinolines: chloroquine, quinidine, lumefantrine, and primaquine. As a positive control, we used the specific inhibitor of purine nucleoside phosphorylase (PNP) proteins, Immucillin H (ImmH), a transition state analog (*41*). Overall, DSF demonstrated that ImmH, quinine, mefloquine, and quinidine exert a dose-dependent stabilizing effect, increasing T_m at 100 μM by 25°C for ImmH, 17.3°C for quinine, 11.2°C for mefloquine, and 1.5°C for quinidine, respectively (Fig. 5A). No change in the protein stability was detected in the presence of chloroquine, lumefantrine, or primaquine at ≤100 μM. To complement the DSF analysis, we investigated the affinity and binding kinetics of quinine and mefloquine with the recombinant PfPNP using surface plasmon resonance (SPR) (Fig. 5, B and C). Association and dissociation rates of the three compounds were measured using single- and multicycle steady-state or kinetic fit experiments (table S2). As expected, ImmH displayed a tight binding and very slow dissociation rate to PfPNP with equilibrium constant (K_D) of about 250 pM, similar to what has previously been reported (i.e., K_D = 860 pM) (Fig. 5B) (*40*). The quinolines have lower affinities to PfPNP, with quinine and mefloquine exhibiting K_D around 30 nM and 40 μM, respectively (Fig. 5, B and C). Last, we validated the observed PfPNP engagement with quinine and mefloquine by isothermal titration calorimetry (ITC). The ITC results were also in good agreement with the SPR results, showing similar binding affinities for quinine (K_D = 65 nM) and mefloquine (K_D = 11 μM) (fig. S7 and table S3). Mixed exothermic and endothermic enthalpy observed upon quinine binding to PfPNP may suggest a secondary binding event of unknown origin with K_D an order of magnitude higher (i.e., ~534 nM).

Next, we used an in vitro enzymatic assay, monitoring PfPNP-catalyzed conversion of inosine to hypoxanthine (*41*, *42*), to investigate the inhibitory effect of quinine and mefloquine on PfPNP. Both drugs blocked the PfPNP enzymatic activity, with the inhibitory constants (K_i) of 138 nM for quinine and 5.9 μM for mefloquine (Fig. 5D and table S4). This effect is somewhat weaker when compared with previously reported K_i of ImmH (i.e., K_i = 29 nM and slow-onset K_i^* = 0.6 nM) (*41*). However, these values correlate with affinities from SPR and ITC, showing that both quinine and mefloquine interact with PfPNP, albeit with lower affinities than for ImmH. Of the two antimalarial compounds, quinine exhibits a consistently higher affinity to PfPNP and increased inhibitory activity, which is also reflected in the initial ITDR CETSA measurements. It is therefore likely that inhibition of PfPNP is relevant for the MoA of quinine, whereas the clinical relevance of the PfPNP interaction with mefloquine is likely less pertinent. To examine this possibility, we evaluated the antimalarial activity of both drugs in combination with ImmH in *P. falciparum* in vitro cultures. We used isobologram

Downloaded from http://stm.sciencemag.org/ by guest on February 8, 2019

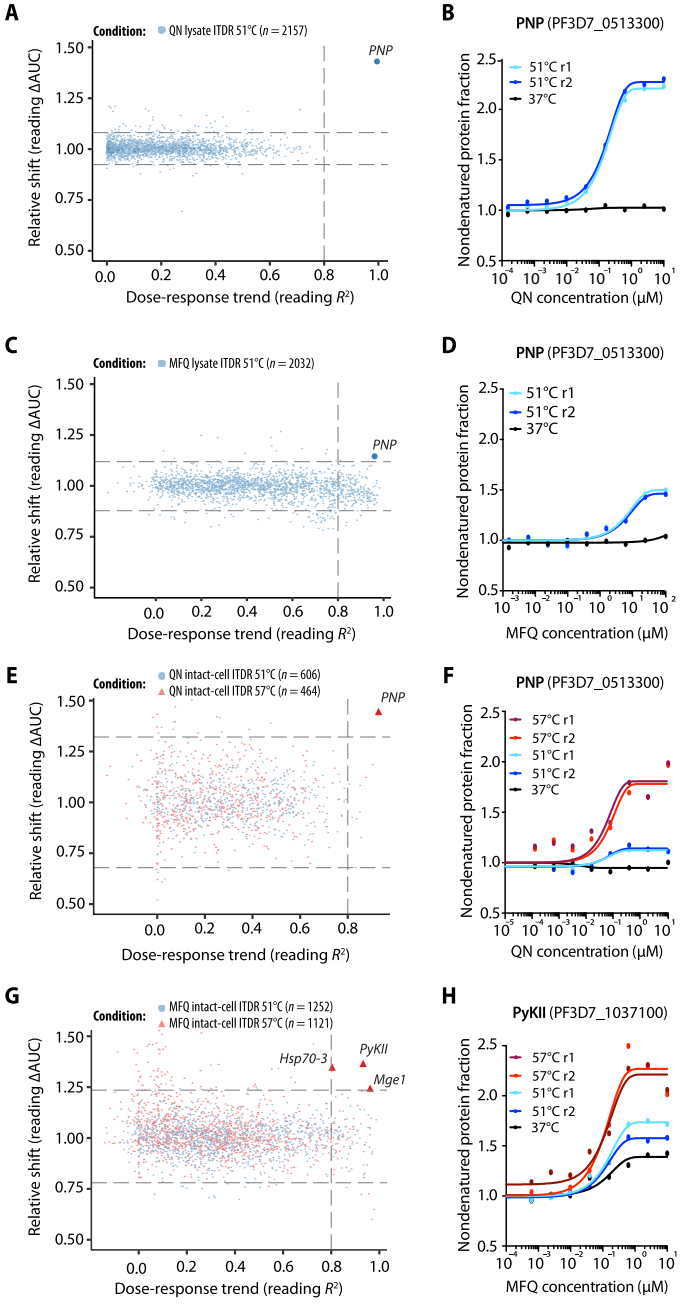

Fig. 4. Deorphanization of quinine and mefloquine protein targets. (**A**) Whole proteome ITDR analysis of quinine-treated (10 to 0 μM) lysate samples, plotted as a function of R^2 against ΔAUC for all proteins ("*n*") detected in the 51°C thermal challenge condition dataset (blue dots) and the reference. The MAD × 3 of ΔAUC and $R^2 = 0.8$ cutoffs are indicated, and stabilized proteins are highlighted. (**B**) Protein stabilization profile of the top drug-binding candidate identified in the preceding panel. The extent of stabilization (*y* axis), depicted as the remaining soluble protein abundance after thermal challenge [51°C (blue)] relative to the no-drug control is plotted along the drug gradient (*x* axis). The nondenaturing 37°C control condition is plotted in black. Subsequent panel pairs represent the results of corresponding ITDR analyses, depicted and described as in (A) and (B), but conducted for: mefloquine (0 to 100 μM) in lysate in (**C**) and (**D**); quinine (0 to 10 μM) in intact-cell in (**E**) and (**F**); mefloquine (0 to 10 μM) in intact-cell in (**G**) and (**H**). All intact-cell analyses have an additional 57°C thermal challenge condition (red triangles). The stabilization curves for the two additional hits identified in mefloquine intact-cell ITDR 57°C but not represented in (H) are listed in the fig. S4.

analysis, a classical graphical drug interaction evaluation method to uncover synergistic and/or antagonistic effects among the drug pairs that could signal a common target (*43*). In assembled isobolograms, both quinolines induced a lower killing effect (quinine, $\Sigma FIC_{50} \leq 1.43$; mefloquine, $\Sigma FIC_{50} \leq 1.70$) when in combination with ImmH, than it would be expected if their effects were additive ($\Sigma FIC_{50} = 1$) (Fig. 5E and table S5). A substantial skewing of both isoboles can be observed across the drug ratios tested, which is indicative of drug antagonism. In contrast, the isobologram of ImmH combination with E64d, which is not expected to interact with PfPNP, shows markedly lower amplitude of deviation from the linear function (mean $\Sigma FIC_{50} = 1.09$), suggesting additive independent activities. Because PfPNP is the only known common target of ImmH and the two quinoline drugs, the observed antagonistic effect is likely caused by the competition for binding to the PfPNP active site.

Crystal structure of mefloquine and quinine bound to PfPNP

To shed further light on the mode of inhibition of PfPNP, we determined cocrystal structures of the protein with quinine and mefloquine at resolutions of 1.66 and 2.30 Å, respectively. The structures show both compounds bind in the active site pocket of PfPNP (Fig. 6, A and B), consistent with their effective inhibition of the enzymatic activity. The observed folds of PfPNP in the cocrystallized PfPNP-quinine and PfPNP-mefloquine complexes are highly similar, as indicated by low-degree variability in atom positioning between the two structures [i.e., root mean square deviation (RMSD) of C alpha atoms of 0.2 Å]. The overall structures are also very similar to previously determined complexes of PfPNP-inosine (RMSD, 0.34/0.41 Å) (*44*) and PfPNP-ImmH·SO_4 (RMSD, 0.24/0.28 Å) (*40*) (fig. S8). An exception is the active site loop Trp^{212}-Val^{222} of PfPNP, which is not well defined in the electron density of the PfPNP-mefloquine complex. The disordering of this loop region can be explained by potential steric hindrance of the mefloquine trifluoromethyl moiety with the side chain of Trp^{212}, which in the PfPNP-inosine and PfPNP-quinine structures extends into this region of the active site. The ring system of quinine is positioned in a similar manner to the heterocyclic aromatic rings of inosine, whereas the mefloquine ring system is flipped 180° with a smaller overlap with the inosine position. A key determinant for binding of both compounds is the "shoe-like" shape of the pocket with a flat bottom formed by the side chain of Val^{181} and several β strand main-chain moieties and where Tyr^{160} forms a hydrophobic lacing from the top (Fig. 6, C and D). In the quinine structure, Trp^{212} constitutes an additional hydrophobic lace for the aromatic moiety of quinine.

The binding pocket for the compounds contains both polar and hydrophobic moieties, but except for the stacking interactions, there are no conserved protein interactions with the aromatic system in the two compounds. The quinuclidine moiety of quinine is positioned in the region of the ribose in the PfPNP-inosine complex, and a stabilizing hydrogen bond is made by the protonated nitrogen of quinine quinuclidine ring with the α-carboxylic group of Asp^{218} (2.7 Å). In both the quinine and mefloquine structures, a phosphate ion is bound in the same region as the leaving phosphate ion of the enzyme-inosine product complex. This phosphate is likely essential for the binding of the two compounds when it shields the highly positive charge of this region within the pocket. Although mefloquine is added to the crystal as a racemic mixture, only the (+)-mefloquine enantiomer binds to the active site of the PfPNP (Fig. 6E). This is consistent with previous data supporting a stronger

Downloaded from http://stm.sciencemag.org/ by guest on February 8, 2019

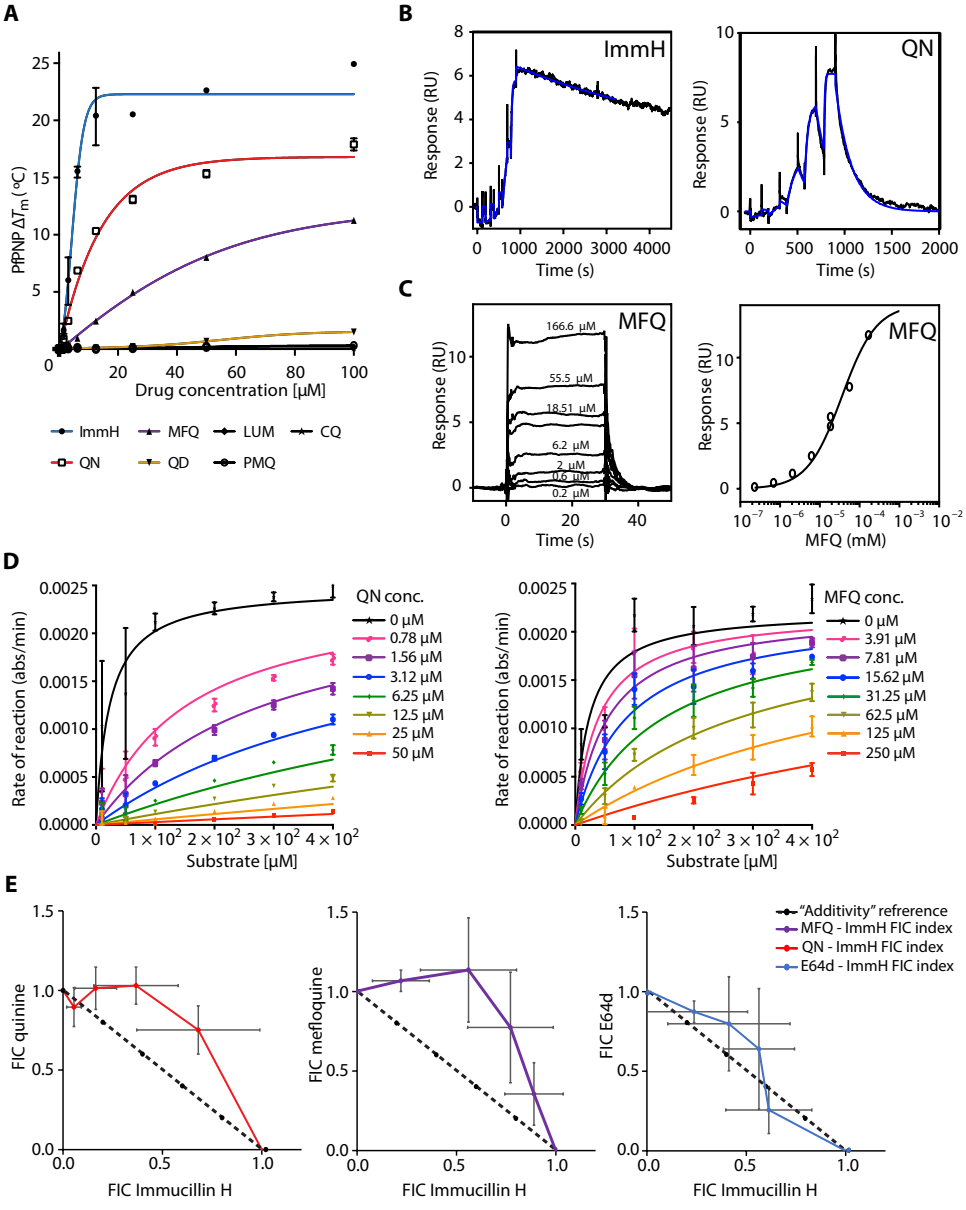

Fig. 5. Validation of PfPNP as a target of quinine and mefloquine. (**A**) DSF analysis of PfPNP stabilization by ImmH, mefloquine (MFQ), quinine (QN), quinidine (QD), lumefantrine (LUM), chloroquine (CQ), and primaquine (PMQ) in a concentration gradient (0 to 100 μM). The change in PfPNP T_m under drug exposure relative to untreated sample is represented on the *y* axis in relation to drug concentration. (**B** and **C**) Sensorgrams, double-referenced binding data (black traces) and fitted (blue traces) from SPR analysis of PfPNP binding affinity to three drugs. ImmH and quinine (B) were analyzed using single-cycle experiments and kinetic 1-to-1 model, whereas mefloquine (C) was analyzed in a multicycle experiment and fitted using a steady-state model. Mefloquine binding isotherm is represented below the sensorgram. (**D**) PfPNP enzymatic activity inhibition by quinine and mefloquine across 0 to 50 μM and 0 to 250 μM drug concentration gradients, respectively. (**E**) Fractional inhibitory concentration 50 (FIC) analysis for the combinations of ImmH with mefloquine, quinine, and E64d. Isoboles representing FIC index of each drug in combination are plotted across a range of drug pair concentrations. Reference isobole indicating Loewe additivity model is presented as a black dashed line.

antiplasmodial activity of (+) enantiomer (*45*) and further supports that the PfPNP inhibition contributes to the antimalarial activity of mefloquine.

DISCUSSION

Plasmodium parasites are characterized by unique biology combining both animal- and plant-like features and thus remain poorly understood compared with other eukaryotic systems. Hence, research tools developed for studies of drug activities in other eukaryotic systems have been applied to studying these protozoa with limited success (*46*). As a result, our understanding of the MoAs of the vast majority of antimalarial drugs remains fragmentary even for compounds that have been in clinical use for multiple decades (*7*, *10*). Here, we explored the CETSA approach for identification of protein targets of antimalarial compounds directly in the *P. falciparum* cells.

In other eukaryotic cellular systems, CETSA was proven useful for the identification of direct drug targets (*20*, *47*, *48*), downstream effects of the drug-induced perturbations (*19*), and drug resistance mechanisms (*49*) and was also shown to be a powerful readout tool in compound library screenings (*50*). Here, we first demonstrated its capacity to detect the known targets of pyrimethamine and E64d in the main malaria pathogen *P. falciparum*. Inhibition of PfDHFR-TS was directly linked to the parasiticidal effect of pyrimethamine (*27*, *28*), and multiple in vitro and clinical studies have provided further support for this interaction (*51*–*53*). This makes the MoA of pyrimethamine one of the most well characterized among all antimalarial drugs. Nonetheless, using CETSA, we demonstrate that pyrimethamine binds PfDHFR-TS as the only target in the proteome covered, resulting in its thermal stabilization in the lysate ITDR experiment. However, the ITDR and melt curve experiments with pyrimethamine in intact cells yielded no stabilization of PfDHFR-TS, illustrating that certain binding scenarios can mask CETSA shifts under specific conditions. This could reflect a reduced affinity of pyrimethamine to the DHFR active site within the cell, being outcompeted by a high-affinity ligand such as folate. Conversely, the drug-target engagement in intact cells was demonstrated for E64d, a cell-permeable synthetic analog of an epoxysuccinyl-based cysteine protease inhibitor E64. E64d is known to be hydrolyzed to its active form (E64c) by intracellular esterases before covalently binding to the sulfhydryl group at the active site of the target protease (*54*, *55*). Accordingly, in the intact-cell ITDR analysis, we demonstrated that E64d induced thermal stabilization of several predicted

Downloaded from http://stm.sciencemag.org/ by guest on February 8, 2019

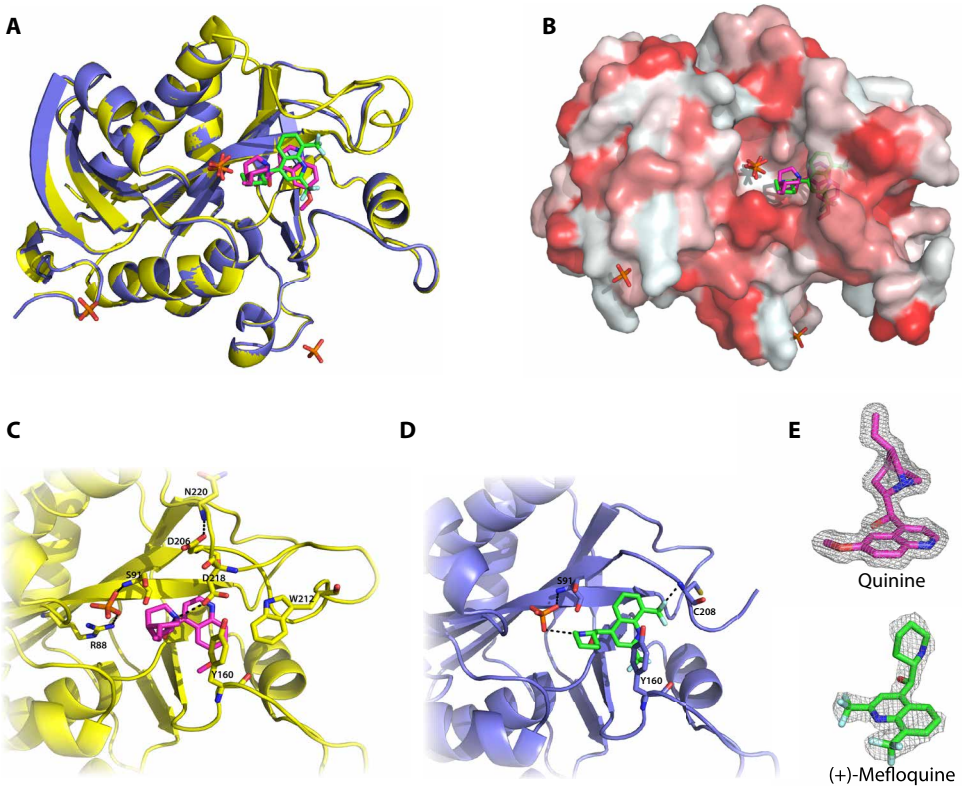

Fig. 6. Cocrystal structures of PfPNP with quinine and mefloquine. (**A**) Overlay of PFPNP-quinine·PO_4 and PfPNP-mefloquine·PO_4 cocrystal structures. Quinine is represented as pink sticks, mefloquine as green sticks, and the two corresponding protein structures in yellow and blue, respectively. Oxygen, blue; phosphorus, orange; oxygen, red; fluorine, light cyan. (**B**) Surface representation of both structures, showing hydrophobic (red) regions and both ligands bound to PfPNP. (**C** and **D**) Magnified binding pockets of structures presented in (A); major interactions between ligands and binding pocket amino acids are represented by black dashed lines. (**E**) Fo-Fc electron density maps of quinine and mefloquine residing within binding pockets of the two cocrystal structures contoured at 1σ level.

cysteine proteases including its previously known targets FP2 and FP3 (*31*–*33*). In addition, the drug interacted with DPAP1, a *P. falciparum* ortholog of mammalian cathepsin C that was also implicated in hemoglobin catabolism and was shown to be critical for the parasite's asexual growth (*56*). This illustrates CETSA's ability to detect the drug-target binding that may occur only in the intact-cell setting but not in parasite lysate. This may reflect possible prerequisites for drug interactions that occur only in the context of an intact cell such as drug activation after cell entry, presence of cofactors, or accumulation of a drug at a specific subcellular compartment or an appropriate local environment. Consequently, not all drug targets are necessarily identified in CETSA analysis, either due to finite depth of proteomic analysis or the lack of observable thermal stabilization at temperatures or conditions chosen for the experiment. To maximize the method's detection capacity for drugs with uncharacterized MoA, it is advantageous to use both lysate- and intact cell–based CETSA formats. It is particularly important, considering that not all thermal stability shifts are direct results of drug binding, but they can also be caused by downstream effects including changes in protein stability due to binding of physiological ligands such as metabolites, nucleic acids, or proteins. Such shifts could be due to modulation of cell signaling, metabolism, or stress pathways induced by the drug. Cross-referencing of the lysate and intact-cell CETSA datasets provides one of the avenues for differentiating between direct and indirect drug effects. Furthermore, the predominantly insoluble nature of membrane proteins (*57*), or their presence in soluble lipid bilayer particles generated during cell lysis, results in their limited propensity for observable thermal shifts in the current version of the CETSA protocol (*21*). Future applications of this method for *Plasmodium* parasites might also explore the use of mild detergents (*58*), aiming to increase the coverage of the membrane proteome.

Quinine and mefloquine appear to have overlapping MoAs involving multiple biological functions in the *Plasmodium* cell (*7*) such as hemoglobin endocytosis (*59*) and heme detoxification (*60*). However, the two drugs have also been suggested to have unique features, such as intercalation with DNA by quinine (*61*) and translation inhibition by mefloquine (*17*). Overall, the MoAs of both drugs appear to involve disruption of several biological processes simultaneously, but for quinine, no direct protein targets have been previously identified. Conversely, a direct interaction of mefloquine with the 80*S* ribosome was recently suggested, resulting in attenuation of parasite protein synthesis (*17*). Here, we show that quinine and mefloquine interact with PfPNP in the *Plasmodium* cell and that both drugs have the capacity to inhibit PfPNP's enzymatic activity. Although quinine and mefloquine exhibited comparable thermal stabilization of PfPNP in the initial lysate-based CETSA (MDT ~0.1 μM for quinine and ~0.6 μM for mefloquine), in the follow-up studies, quinine exhibited up to three orders of the magnitude higher affinity to this enzyme. In particular, quinine was able to inhibit PfPNP enzymatic activity with a binding constant K_i ~140 nM, which indicates its potential as a clinically relevant activity. PfPNP is a dual specificity enzyme important for the salvage and recycling of purines (*39*, *41*). However, its relevance as an antimalarial target is complicated by the presence of the human PNP homologue in the RBC in micromolar concentrations, which results in the parasite being capable of scavenging its downstream metabolic products (*62*, *63*). The disruption of the *pfpnp* gene appears to increase the parasite's requirement for purines and is lethal at physiological hypoxanthine levels in vitro (*64*). PNP is also essential for parasite fitness and pathogenicity in the *Plasmodium yoelii* rodent model (*65*) but seems nonessential in the *Plasmodium berghei* ANKA model (*66*). Strong evidence in support of PNP importance as a drug target was generated from a nonhuman primate *P. falciparum* infection model, demonstrating clinical efficacy of orally administered DADMe-Immucillin-G, an inhibitor of both human and plasmodium PNPs (*67*). Drug treatment provoked parasite clearance in otherwise lethal infection in *Aeotus* monkeys, although some recrudescence was observed (*67*). More recently, it was shown that prolonged exposure of *P. falciparum* to sublethal concentrations of

Downloaded from http://stm.sciencemag.org/ by guest on February 8, 2019

DADMe-Immucillin-G in vitro results in resistance, mediated by point mutations in the catalytic site of PfPNP and the mutant gene copy number amplification (*68*). This study supported previous findings that inhibition of PfPNP is crucial for the antimalarial effect of immucillins (*39*, *40*, *69*). Another immucillin derivative, MT-ImmH, exhibiting 100-fold higher affinity for the parasite enzyme (*40*) displayed an antimalarial median inhibitory concentration (IC_{50}) in in vitro assays within the nanomolar range but did not completely attenuate parasite growth below micromolar concentrations (*39*, *40*). Together, these reports collectively suggest that the inhibition of PfPNP has a high potential for antiplasmodial activity either as a direct killing mechanism and/or by decreasing parasite's fitness. The high-affinity binding and inhibition of enzymatic activity suggest that PfPNP may particularly contribute to the MoA of quinine.

The antagonistic interactions observed between the cytotoxic effects of quinine and mefloquine with ImmH support the notion that PfPNP inhibition contributes to their antimalarial activity. However, although immucillins exert their antimalarial effect through simultaneous inhibition of host and parasite PNP enzymes, we found no evidence that quinine and mefloquine interact with human PNP. The structure of the binding pocket of two crystal structures resolved in this study is very similar to previously described PfPNP structures (*40*, *44*). The cocrystal structure of PfPNP-ImmH determined by Cassera and colleagues (*67*) revealed a large solvent-filled pocket within the enzyme's active site located near the 5′-hydroxyl group of ImmH. This structural feature distinguishes the *P. falciparum* enzyme from its human counterpart, resulting in distinct substrate binding specificities between the two (*67*) and could be responsible for the interaction with the quinoline compounds or the lack thereof. Nevertheless, we suggest that the described quinine-PfPNP interaction, and possibly the mefloquine-PfPNP interaction, is additive to their antimalarial effects rather than representing their dominant MoA. Other killing mechanisms might be more pronounced at concentrations required to kill the parasite in the in vitro assay conditions. Moreover, in the clinical setting, both quinoline methanols remain in circulation for prolonged periods of time either due to a very long half-life (mefloquine) or repetitive administration (quinine) (*11*). Hence, the negative impact of a prolonged PfPNP inhibition on parasite fitness could also contribute to their therapeutic effect in vivo. Moreover, PfPNP was identified as the most prominent target of quinine in the mid-stage of the *Plasmodium* intraerythrocytic developmental cycle, the trophozoite stage, which is known to be highly sensitive to quinine (*70*). However, we cannot rule out the possibility that another therapeutic target of quinine exists in this or other stages of the asexual intraerythrocytic development, such as the schizonts.

The need of new therapeutics for malaria becomes particularly urgent in the light of emerging artemisinin resistance (*3*). High-throughput phenotypic screens conducted by collaborative efforts of the public and private sectors tested millions of compounds yielding tens of thousands of molecules with <1 μM activity against different developmental stages of *P. falciparum* (*71*, *72*). One of the main remaining challenges is the identification of intrinsic molecular targets for the most potent compounds while prioritizing radically new chemotypes. New technologies developed for *P. falciparum* over the past few years have enhanced our capacity to identify and validate candidate drug targets. However, MS-CETSA offers several advantages over existing tools for drug target identification. Its capacity to monitor direct biophysical binding to protein targets within a large fraction of the parasite proteome simultaneously makes it suitable for identification of drug targets of compounds with previously undetermined modes of action. The label-free principle of CETSA allows its usage with the parasite strain of choice and standard unmodified compounds, thus reducing time and cost required for the synthesis of special drug probes. It is our belief that the development of MS-CETSA for *P. falciparum* can complement existing tools, facilitating antimalarial drug target discovery efforts, and serve to further deepen our understanding of parasite biology.

MATERIALS AND METHODS

Study design

The study was designed to adapt the MS-CETSA method for malaria research and explore its application for stringent identification of antimalarial drug targets in the *P. falciparum* proteome. Initially, we used the melt curve MS-CETSA to characterize the thermal denaturation behavior of the *P. falciparum* proteome. Subsequently, we provided proof of principle for the drug target identification using an ITDR MS-CETSA variant, using two compounds with known molecular targets in the *P. falciparum* proteome: pyrimethamine and E64d. We then used ITDR to identify PfPNP as a new binding partner of two clinically used compounds: quinine and mefloquine. Drug-target interactions were validated and characterized through biochemical and cellular studies including DSF, ITC, SPR, enzymatic activity assays, antimalarial activity synergy assays, and x-ray crystallography. All CETSA experiments were carried out in two technical replicates, whereas biochemical and cellular assays were carried out in biological triplicates unless indicated otherwise.

Statistical analysis

In general, all data points are shown in the respective figures. Briefly, all CETSA ITDR data were fitted using a sigmoidal (variable slope) curve fit. Each protein stabilization profile was evaluated for the dose-response curve best-fitting quality (expressed as R^2), the level of stabilization in heat-challenged condition relative to nondenaturing conditions of 37°C calculated as the difference in AUC and the protein abundance fold change relative to drug-free/dimethyl sulfoxide (DMSO)–vesicle condition. The criteria used for high-confidence stabilization candidates are characterized by $R^2 \geq 0.8$, ΔAUC surpassing three times of MAD of the baseline distribution, and fold change ≥1.3 (i.e., 30% change) in the relative protein abundance in at least one drug dose–treated sample relative to a DMSO-treated sample. Where applicable, further details of statistical analysis and the methods used are described elsewhere in Supplementary Materials and Methods.

SUPPLEMENTARY MATERIALS

www.sciencetranslationalmedicine.org/cgi/content/full/11/473/eaau3174/DC1

Materials and Methods

Fig. S1. Coaggregation of protein complexes in *P. falciparum* melt curve CETSA.

Fig. S2. The comparison of protein melting behavior between RBC, *P. falciparum*, and K562 cells.

Fig. S3. The effect of pyrimethamine on thermal stability of PfDHFR-TS across four CETSA experimental variants.

Fig. S4. Mefloquine-induced stabilization profiles of Mge1 and Hsp70-3 in intact-cell ITDR assay.

Fig. S5. Western blot detection of PfPNP stabilization in mefloquine- and quinine-treated ITDR datasets.

Fig. S6. Human protein engagement by antimalarial drugs in intact-cell ITDR assays.

Fig. S7. ITC analysis of quinine and mefloquine binding to PfPNP.

Downloaded from http://stm.sciencemag.org/ by guest on February 8, 2019

Fig. S8. Cocrystal structure overlay with 2bsx and 1nw4 reference PfPNP structures.
Table S1. High- and low-confidence protein stabilizations observed in quinine/mefloquine ITDR assays.
Table S2. SPR measurements of PfPNP-mefloquine/quinine/ImmH K_D.
Table S3. ITC binding affinities for PfPNP-mefloquine/quinine interaction.
Table S4. PfPNP in vitro enzymatic activity inhibition by mefloquine and quinine.
Table S5. Combinatory effect of fixed-ratio drug combinations against *P. falciparum* 3D7 strain.
Table S6. Data collection and refinement statistics of PfPNP-mefloquine and PfPNP-quinine cocrystals.
Data S1. Intact-cell and lysate CETSA melt curve analysis of *P. falciparum* proteome.
Data S2. Intact-cell CETSA melt curve analysis of RBC proteome.
Data S3. PM lysate ITDR–plasmodium proteome.
Data S4. E64d intact-cell ITDR–plasmodium proteome.
Data S5. Quinine lysate ITDR–plasmodium proteome.
Data S6. Mefloquine lysate ITDR–plasmodium proteome.
Data S7. Quinine intact-cell ITDR–plasmodium proteome.
Data S8. Quinine intact-cell ITDR–human proteome.
Data S9. Mefloquine intact-cell ITDR–plasmodium proteome.
Data S10. Mefloquine intact-cell ITDR–human proteome.
References (*73*–*81*)

REFERENCES AND NOTES

1. WHO, *World Malaria Report 2017* (WHO, 2017).
2. WHO, *Implications of Insecticide Resistance for Malaria Vector Control* (WHO, 2016).
3. A. M. Dondorp, F. Nosten, P. Yi, D. Das, A. P. Phyo, J. Tarning, K. M. Lwin, F. Ariey, W. Hanpithakpong, S. J. Lee, P. Ringwald, K. Silamut, M. Imwong, K. Chotivanich, P. Lim, T. Herdman, S. S. An, S. Yeung, P. Singhasivanon, N. P. J. Day, N. Lindegardh, D. Socheat, N. J. White, Artemisinin resistance in *Plasmodium falciparum* malaria. *N. Engl. J. Med.* **361**, 455–467 (2009).
4. WHO, Geneva, Status report on artemisinin and ACT resistance (April 2017) *WHO* (2017); www.who.int/malaria/publications/atoz/artemisinin-resistance-april2017/en/).
5. N. J. White, Antimalarial drug resistance. *J. Clin. Invest.* **113**, 1084–1092 (2004).
6. D. A. Fidock, P. J. Rosenthal, S. L. Croft, R. Brun, S. Nwaka, Antimalarial drug discovery: Efficacy models for compound screening. *Nat. Rev. Drug Discov.* **3**, 509–520 (2004).
7. M. Foley, L. Tilley, Quinoline antimalarials mechanisms of action and resistance and prospects for new agents. *Pharmacol. Ther.* **79**, 55–87 (1998).
8. D. J. Sullivan Jr., I. Y. Gluzman, D. G. Russell, D. E. Goldberg, On the molecular mechanism of chloroquine's antimalarial action. *Proc. Natl. Acad. Sci. U.S.A.* **93**, 11865–11870 (1996).
9. P. G. Bray, S. A. Ward, P. M. O'Neill, Quinolines and artemisinin: Chemistry, biology and history. *Curr. Top. Microbiol. Immunol.* **295**, 3–38 (2005).
10. F. W. Muregi, Antimalarial drugs and their useful therapeutic lives: Rational drug design lessons from pleiotropic action of quinolines and artemisinins. *Curr. Drug Discov. Technol.* **7**, 280–316 (2010).
11. WHO, Geneva, Guidelines for the treatment of malaria - 3rd edition (2015); http://apps.who.int/iris/bitstream/10665/162441/1/9789241549127_eng.pdf.
12. L. W. Kitchen, D. W. Vaughn, D. R. Skillman, Role of US military research programs in the development of US food and drug administration–approved antimalarial drugs. *Clin. Infect. Dis.* **43**, 67–71 (2006).
13. P. Schlagenhauf, M. Adamcova, L. Regep, M. T. Schaerer, H.-G. Rhein, The position of mefloquine as a 21st century malaria chemoprophylaxis. *Malar. J.* **9**, 357 (2010).
14. A. M. Thu, A. P. Phyo, J. Landier, D. M. Parker, F. H. Nosten, Combating multidrug-resistant *Plasmodium falciparum* malaria. *FEBS J.* **284**, 2569–2578 (2017).
15. M. B. Reed, K. J. Saliba, S. R. Caruana, K. Kirk, A. F. Cowman, Pgh1 modulates sensitivity and resistance to multiple antimalarials in *Plasmodium falciparum*. *Nature* **403**, 906–909 (2000).
16. S. R. Karcz, D. Galatis, A. F. Cowman, Nucleotide binding properties of a P-glycoprotein homologue from *Plasmodium falciparum*. *Mol. Biochem. Parasitol.* **58**, 269–276 (1993).
17. W. Wong, X.-C. Bai, B. E. Sleebs, T. Triglia, A. Brown, J. K. Thompson, K. E. Jackson, E. Hanssen, D. S. Marapana, I. S. Fernandez, S. A. Ralph, A. F. Cowman, S. H. W. Scheres, J. Baum, Mefloquine targets the *Plasmodium falciparum* 80S ribosome to inhibit protein synthesis. *Nat. Microbiol.* **2**, nmicrobiol201731 (2017).
18. P. Olliaro, Mode of action and mechanisms of resistance for antimalarial drugs. *Pharmacol. Ther.* **89**, 207–219 (2001).
19. D. M. Molina, P. Nordlund, The cellular thermal shift assay: A novel biophysical assay for in situ drug target engagement and mechanistic biomarker studies. *Annu. Rev. Pharmacol. Toxicol.* **56**, null (2016).
20. D. M. Molina, R. Jafari, M. Ignatushchenko, T. Seki, E. A. Larsson, C. Dan, L. Sreekumar, Y. Cao, P. Nordlund, Monitoring drug target engagement in cells and tissues using the cellular thermal shift assay. *Science* **341**, 84–87 (2013).
21. M. M. Savitski, F. B. M. Reinhard, H. Franken, T. Werner, M. F. Savitski, D. Eberhard, D. M. Molina, R. Jafari, R. B. Dovega, S. Klaeger, B. Kuster, P. Nordlund, M. Bantscheff, G. Drewes, Tracking cancer drugs in living cells by thermal profiling of the proteome. *Science* **346**, 1255784 (2014).
22. U. B. Ericsson, B. M. Hallberg, G. T. Detitta, N. Dekker, P. Nordlund, Thermofluor-based high-throughput stability optimization of proteins for structural studies. *Anal. Biochem.* **357**, 289–298 (2006).
23. E. M. Pasini, M. Kirkegaard, P. Mortensen, H. U. Lutz, A. W. Thomas, M. Mann, In-depth analysis of the membrane and cytosolic proteome of red blood cells. *Blood* **108**, 791–801 (2006).
24. L. Dai, T. Zhao, X. Bisteau, W. Sun, N. Prabhu, Y. T. Lim, R. M. Sobota, P. Kaldis, P. Nordlund, Modulation of protein-interaction states through the cell cycle. *Cell* **173**, 1481–1494.e13 (2018).
25. B. N. Pease, E. L. Huttlin, M. P. Jedrychowski, E. Talevich, J. Harmon, T. Dillman, N. Kannan, C. Doerig, R. Chakrabarti, S. P. Gygi, D. Chakrabarti, Global analysis of protein expression and phosphorylation of three stages of *Plasmodium falciparum* intraerythrocytic development. *J. Proteome Res.* **12**, 4028–4045 (2013).
26. C. S. H. Tan, K. D. Go, X. Bisteau, L. Dai, C. H. Yong, N. Prabhu, M. B. Ozturk, Y. T. Lim, L. Sreekumar, J. Lengqvist, V. Tergaonkar, P. Kaldis, R. M. Sobota, P. Nordlund, Thermal proximity coaggregation for system-wide profiling of protein complex dynamics in cells. *Science* **359**, 1170–1177 (2018).
27. A. F. Cowman, M. J. Morry, B. A. Biggs, G. A. Cross, S. J. Foote, Amino acid changes linked to pyrimethamine resistance in the dihydrofolate reductase-thymidylate synthase gene of *Plasmodium falciparum*. *Proc. Natl. Acad. Sci. U.S.A.* **85**, 9109–9113 (1988).
28. D. S. Peterson, D. Walliker, T. E. Wellems, Evidence that a point mutation in dihydrofolate reductase-thymidylate synthase confers resistance to pyrimethamine in falciparum malaria. *Proc. Natl. Acad. Sci. U.S.A.* **85**, 9114–9118 (1988).
29. L. Vivas, L. Rattray, L. B. Stewart, B. L. Robinson, B. Fugmann, R. K. Haynes, W. Peters, S. L. Croft, Antimalarial efficacy and drug interactions of the novel semi-synthetic endoperoxide artemisone in vitro and in vivo. *J. Antimicrob. Chemother.* **59**, 658–665 (2007).
30. Y. Yuthavong, B. Tarnchompoo, T. Vilaivan, P. Chitnumsub, S. Kamchonwongpaisan, S. A. Charman, D. N. McLennan, K. L. White, L. Vivas, E. Bongard, C. Thongphanchang, S. Taweechai, J. Vanichtanankul, R. Rattanajak, U. Arwon, P. Fantauzzi, J. Yuvaniyama, W. N. Charman, D. Matthews, Malarial dihydrofolate reductase as a paradigm for drug development against a resistance-compromised target. *Proc. Natl. Acad. Sci. U.S.A.* **109**, 16823–16828 (2012).
31. I. D. Kerr, J. H. Lee, K. C. Pandey, A. Harrison, M. Sajid, P. J. Rosenthal, L. S. Brinen, Structures of falcipain-2 and falcipain-3 bound to small molecule inhibitors: Implications for substrate specificity. *J. Med. Chem.* **52**, 852–857 (2009).
32. B. R. Shenai, P. S. Sijwali, A. Singh, P. J. Rosenthal, Characterization of native and recombinant falcipain-2, a principal trophozoite cysteine protease and essential hemoglobinase of *Plasmodium falciparum*. *J. Biol. Chem.* **275**, 29000–29010 (2000).
33. S. C. Xie, C. Dogovski, E. Hanssen, F. Chiu, T. Yang, M. P. Crespo, C. Stafford, S. Batinovic, S. Teguh, S. Charman, N. Klonis, L. Tilley, Haemoglobin degradation underpins the sensitivity of early ring stage *Plasmodium falciparum* to artemisinins. *J. Cell Sci.* **129**, 406–416 (2016).
34. P. S. Sijwali, K. Kato, K. B. Seydel, J. Gut, J. Lehman, M. Klemba, D. E. Goldberg, L. H. Miller, P. J. Rosenthal, *Plasmodium falciparum* cysteine protease falcipain-1 is not essential in erythrocytic stage malaria parasites. *Proc. Natl. Acad. Sci. U.S.A.* **101**, 8721–8726 (2004).
35. M. Chan, D. S. H. Tan, T. S. Sim, *Plasmodium falciparum* pyruvate kinase as a novel target for antimalarial drug-screening. *Travel Med. Infect. Dis.* **5**, 125–131 (2007).
36. M. Zhang, C. Wang, T. D. Otto, J. Oberstaller, X. Liao, S. R. Adapa, K. Udenze, I. F. Bronner, D. Casandra, M. Mayho, J. Brown, S. Li, J. Swanson, J. C. Rayner, R. H. Y. Jiang, J. H. Adams, Uncovering the essential genes of the human malaria parasite *Plasmodium falciparum* by saturation mutagenesis. *Science* **360**, eaap7847 (2018).
37. S. Gunjan, S. K. Singh, T. Sharma, H. Dwivedi, B. S. Chauhan, M. I. Siddiqi, R. Tripathi, Mefloquine induces ROS mediated programmed cell death in malaria parasite: *Plasmodium*. *Apoptosis* **21**, 955–964 (2016).
38. P. E. Daddona, W. P. Wiesmann, W. Milhouse, J. W. Chern, L. B. Townsend, M. S. Hershfield, H. K. Webster, Expression of human malaria parasite purine nucleoside phosphorylase in host enzyme-deficient erythrocyte culture. Enzyme characterization and identification of novel inhibitors. *J. Biol. Chem.* **261**, 11667–11673 (1986).
39. L.-M. Ting, W. Shi, A. Lewandowicz, V. Singh, A. Mwakingwe, M. R. Birck, E. A. T. Ringia, G. Bench, D. C. Madrid, P. C. Tyler, G. B. Evans, R. H. Furneaux, V. L. Schramm, K. Kim, Targeting a novel *Plasmodium falciparum* purine recycling pathway with specific immucillins. *J. Biol. Chem.* **280**, 9547–9554 (2005).
40. W. Shi, L.-M. Ting, G. A. Kicska, A. Lewandowicz, P. C. Tyler, G. B. Evans, R. H. Furneaux, K. Kim, S. C. Almo, V. L. Schramm, *Plasmodium falciparum* purine nucleoside phosphorylase: Crystal structures, immucillin inhibitors, and dual catalytic function. *J. Biol. Chem.* **279**, 18103–18106 (2004).
41. G. A. Kicska, P. C. Tyler, G. B. Evans, R. H. Furneaux, K. Kim, V. L. Schramm, Transition state analogue inhibitors of purine nucleoside phosphorylase from *Plasmodium falciparum*. *J. Biol. Chem.* **277**, 3219–3225 (2002).

Downloaded from http://stm.sciencemag.org/ by guest on February 8, 2019

42. R. W. Miles, P. C. Tyler, R. H. Furneaux, C. K. Bagdassarian, V. L. Schramm, One-third-the-sites transition-state inhibitors for purine nucleoside phosphorylase. *Biochemistry* **37**, 8615–8621 (1998).
43. M. C. Berenbaum, What is synergy? *Pharmacol. Rev.* **41**, 93–141 (1989).
44. C. Schnick, M. A. Robien, A. M. Brzozowski, E. J. Dodson, G. N. Murshudov, L. Anderson, J. R. Luft, C. Mehlin, W. G. J. Hol, J. A. Brannigan, A. J. Wilkinson, Structures of *Plasmodium falciparum* purine nucleoside phosphorylase complexed with sulfate and its natural substrate inosine. *Acta Crystallogr. D Biol. Crystallogr.* **61**, 1245–1254 (2005).
45. J. M. Karle, R. Olmeda, L. Gerena, W. K. Milhous, *Plasmodium falciparum*: Role of absolute stereochemistry in the antimalarial activity of synthetic amino alcohol antimalarial agents. *Exp. Parasitol.* **76**, 345–351 (1993).
46. K. A. Meissner, S. Lunev, Y.-Z. Wang, M. Linzke, F. de Assis Batista, C. Wrenger, M. R. Groves, Drug target validation methods in malaria—Protein interference assay (PIA) as a tool for highly specific drug target validation. *Curr. Drug Targets* **18**, 1069–1085 (2017).
47. H. Franken, T. Mathieson, D. Childs, G. M. A. Sweetman, T. Werner, I. Tögel, C. Doce, S. Gade, M. Bantscheff, G. Drewes, F. B. M. Reinhard, W. Huber, M. M. Savitski, Thermal proteome profiling for unbiased identification of direct and indirect drug targets using multiplexed quantitative mass spectrometry. *Nat. Protoc.* **10**, 1567 (2015).
48. R. Jafari, H. Almqvist, H. Axelsson, M. Ignatushchenko, T. Lundbäck, P. Nordlund, D. Martinez Molina, The cellular thermal shift assay for evaluating drug target interactions in cells. *Nat. Protoc.* **9**, 2100–2122 (2014).
49. A. Alshareef, H.-F. Zhang, Y.-H. Huang, C. Wu, J. D. Zhang, P. Wang, A. El-Sehemy, M. Fares, R. Lai, The use of cellular thermal shift assay (CETSA) to study Crizotinib resistance in ALK-expressing human cancers. *Sci. Rep.* **6**, 33710 (2016).
50. H. Almqvist, H. Axelsson, R. Jafari, C. Dan, A. Mateus, M. Haraldsson, A. Larsson, D. Martinez Molina, P. Artursson, T. Lundbäck, P. Nordlund, CETSA screening identifies known and novel thymidylate synthase inhibitors and slow intracellular activation of 5-fluorouracil. *Nat. Commun.* **7**, 11040 (2016).
51. J. G. Kublin, F. K. Dzinjalamala, D. D. Kamwendo, E. M. Malkin, J. F. Cortese, L. M. Martino, R. A. G. Mukadam, S. J. Rogerson, A. G. Lescano, M. E. Molyneux, P. A. Winstanley, P. Chimpeni, T. E. Taylor, C. V. Plowe, Molecular markers for failure of sulfadoxine-pyrimethamine and chlorproguanil-dapsone treatment of *Plasmodium falciparum* malaria. *J Infect Dis* **185**, 380–388 (2002).
52. D. Menard, F. Yapou, A. Manirakiza, D. Djalle, M. D. Matsika-Claquin, A. Talarmin, Polymorphisms in pfcrt, pfmdr1, dhfr genes and in vitro responses to antimalarials in *Plasmodium falciparum* isolates from Bangui, Central African Republic. *Am. J. Trop. Med. Hyg.* **75**, 381–387 (2006).
53. J. Yuvaniyama, P. Chitnumsub, S. Kamchonwongpaisan, J. Vanichtanankul, W. Sirawaraporn, P. Taylor, M. D. Walkinshaw, Y. Yuthavong, Insights into antifolate resistance from malarial DHFR-TS structures. *Nat. Struct. Biol.* **10**, 357–365 (2003).
54. H.-H. Otto, T. Schirmeister, Cysteine proteases and their inhibitors. *Chem. Rev.* **97**, 133–172 (1997).
55. J. C. Powers, J. L. Asgian, Ö. D. Ekici, K. E. James, Irreversible inhibitors of serine, cysteine, and threonine proteases. *Chem. Rev.* **102**, 4639–4750 (2002).
56. F. Wang, P. Krai, E. Deu, B. Bibb, C. Lauritzen, J. Pedersen, M. Bogyo, M. Klemba, Biochemical characterization of *Plasmodium falciparum* dipeptidyl aminopeptidase 1. *Mol. Biochem. Parasitol.* **175**, 10–20 (2011).
57. A. E. Rawlings, Membrane proteins: Always an insoluble problem? *Biochem. Soc. Trans.* **44**, 790–795 (2016).
58. F. B. M. Reinhard, D. Eberhard, T. Werner, H. Franken, D. Childs, C. Doce, M. F. Savitski, W. Huber, M. Bantscheff, M. M. Savitski, G. Drewes, Thermal proteome profiling monitors ligand interactions with cellular membrane proteins. *Nat. Methods* **12**, 1129–1131 (2015).
59. A. F. Cowman, D. Galatis, J. K. Thompson, Selection for mefloquine resistance in *Plasmodium falciparum* is linked to amplification of the pfmdr1 gene and cross-resistance to halofantrine and quinine. *Proc. Natl. Acad. Sci. U.S.A.* **91**, 1143–1147 (1994).
60. K. N. Olafson, T. Q. Nguyen, J. D. Rimer, P. G. Vekilov, Antimalarials inhibit hematin crystallization by unique drug–surface site interactions. *Proc. Natl. Acad. Sci. U.S.A.* **114**, 7531–7536 (2017).
61. M. W. Davidson, B. G. Griggs, D. W. Boykin, W. D. Wilson, Molecular structural effects involved in the interaction of quinolinemethanolamines with DNA. Implications for antimalarial action. *J. Med. Chem.* **20**, 1117–1122 (1977).
62. M. J. Downie, K. Kirk, C. B. Mamoun, Purine salvage pathways in the intraerythrocytic malaria parasite *Plasmodium falciparum*. *Eukaryot. Cell* **7**, 1231–1237 (2008).
63. N. B. Quashie, D. Dorin-Semblat, P. G. Bray, G. A. Biagini, C. Doerig, L. C. Ranford-Cartwright, H. P. De Koning, A comprehensive model of purine uptake by the malaria parasite *Plasmodium falciparum*: Identification of four purine transport activities in intraerythrocytic parasites. *Biochem. J.* **411**, 287–295 (2008).
64. D. C. Madrid, L.-M. Ting, K. L. Waller, V. L. Schramm, K. Kim, *Plasmodium falciparum* purine nucleoside phosphorylase is critical for viability of malaria parasites. *J. Biol. Chem.* **283**, 35899–35907 (2008).
65. L.-M. Ting, M. Gissot, A. Coppi, P. Sinnis, K. Kim, Attenuated plasmodium yoelii lacking purine nucleoside phosphorylase confer protective immunity. *Nat. Med.* **14**, 954–958 (2008).
66. M. Niikura, S.-I. Inoue, S. Mineo, Y. Yamada, I. Kaneko, S. Iwanaga, M. Yuda, F. Kobayashi, Experimental cerebral malaria is suppressed by disruption of nucleoside transporter 1 but not purine nucleoside phosphorylase. *Biochem. Biophys. Res. Commun.* **432**, 504–508 (2013).
67. M. B. Cassera, K. Z. Hazleton, E. F. Merino, N. O. III, M.-C. Ho, A. S. Murkin, R. DePinto, J. A. Gutierrez, S. C. Almo, G. B. Evans, Y. S. Babu, V. L. Schramm, *Plasmodium falciparum* parasites are killed by a transition state analogue of purine nucleoside phosphorylase in a primate animal model. *PLOS ONE* **6**, e26916 (2011).
68. R. G. Ducati, H. A. Namanja-Magliano, R. K. Harijan, J. E. Fajardo, A. Fiser, J. P. Daily, V. L. Schramm, Genetic resistance to purine nucleoside phosphorylase inhibition in *Plasmodium falciparum*. *Proc. Natl. Acad. Sci. U.S.A.* **115**, 2114–2119 (2018).
69. G. A. Kicska, P. C. Tyler, G. B. Evans, R. H. Furneaux, V. L. Schramm, K. Kim, Purine-less death in *Plasmodium falciparum* induced by immucillin-H, a transition state analogue of purine nucleoside phosphorylase. *J. Biol. Chem.* **277**, 3226–3231 (2002).
70. T. S. Skinner, L. S. Manning, W. A. Johnston, T. M. E. Davis, In vitro stage-specific sensitivity of *Plasmodium falciparum* to quinine and artemisinin drugs. *Int. J. Parasitol.* **26**, 519–525 (1996).
71. F.-J. Gamo, L. M. Sanz, J. Vidal, C. de Cozar, E. Alvarez, J.-L. Lavandera, D. E. Vanderwall, D. V. S. Green, V. Kumar, S. Hasan, J. R. Brown, C. E. Peishoff, L. R. Cardon, J. F. Garcia-Bustos, Thousands of chemical starting points for antimalarial lead identification. *Nature* **465**, 305–310 (2010).
72. W. A. Guiguemde, A. A. Shelat, D. Bouck, S. Duffy, G. J. Crowther, P. H. Davis, D. C. Smithson, M. Connelly, J. Clark, F. Zhu, M. B. Jiménez-Díaz, M. S. Martinez, E. B. Wilson, A. K. Tripathi, J. Gut, E. R. Sharlow, I. Bathurst, F. El Mazouni, J. W. Fowble, I. Forquer, P. L. McGinley, S. Castro, I. Angulo-Barturen, S. Ferrer, P. J. Rosenthal, J. L. DeRisi, D. J. Sullivan, J. S. Lazo, D. S. Roos, M. K. Riscoe, M. A. Phillips, P. K. Rathod, W. C. Van Voorhis, V. M. Avery, R. K. Guy, Chemical genetics of *Plasmodium falciparum*. *Nature* **465**, 311–315 (2010).
73. M. J. Gardner, N. Hall, E. Fung, O. White, M. Berriman, R. W. Hyman, J. M. Carlton, A. Pain, K. E. Nelson, S. Bowman, I. T. Paulsen, K. James, J. A. Eisen, K. Rutherford, S. L. Salzberg, A. Craig, S. Kyes, M.-S. Chan, V. Nene, S. J. Shallom, B. Suh, J. Peterson, S. Angiuoli, M. Pertea, J. Allen, J. Selengut, D. Haft, M. W. Mather, A. B. Vaidya, D. M. A. Martin, A. H. Fairlamb, M. J. Fraunholz, D. S. Roos, S. A. Ralph, G. I. McFadden, L. M. Cummings, G. M. Subramanian, C. Mungall, J. C. Venter, D. J. Carucci, S. L. Hoffman, C. Newbold, R. W. Davis, C. M. Fraser, B. Barrell, Genome sequence of the human malaria parasite *Plasmodium falciparum*. *Nature* **419**, 498–511 (2002).
74. C. O'Donovan, R. Apweiler, A guide to UniProt for protein scientists. *Methods Mol. Biol.* **694**, 25–35 (2011).
75. S. Gräslund, Structural Genomics Consortium; China Structural Genomics Consortium; Northeast Structural Genomics Consortium, P. Nordlund, J. Weigelt, B. M. Hallberg, J. Bray, O. Gileadi, S. Knapp, U. Oppermann, C. Arrowsmith, R. Hui, J. Ming, S. dhe-Paganon, H. Park, A. Savchenko, A. Yee, A. Edwards, R. Vincentelli, C. Cambillau, R. Kim, S.-H. Kim, Z. Rao, Y. Shi, T. C. Terwilliger, C.-Y. Kim, L.-W. Hung, G. S. Waldo, Y. Peleg, S. Albeck, T. Unger, O. Dym, J. Prilusky, J. L. Sussman, R. C. Stevens, S. A. Lesley, I. A. Wilson, A. Joachimiak, F. Collart, I. Dementieva, M. I. Donnelly, W. H. Eschenfeldt, Y. Kim, L. Stols, R. Wu, M. Zhou, S. K. Burley, J. S. Emtage, J. M. Sauder, D. Thompson, K. Bain, J. Luz, T. Gheyi, F. Zhang, S. Atwell, S. C. Almo, J. B. Bonanno, A. Fiser, S. Swaminathan, F. W. Studier, M. R. Chance, A. Sali, T. B. Acton, R. Xiao, L. Zhao, L. C. Ma, J. F. Hunt, L. Tong, K. Cunningham, M. Inouye, S. Anderson, H. Janjua, R. Shastry, C. K. Ho, D. Wang, H. Wang, M. Jiang, G. T. Montelione, D. I. Stuart, R. J. Owens, S. Daenke, A. Schütz, U. Heinemann, S. Yokoyama, K. Büssow, K. C. Gunsalus, Protein production and purification. *Nat. Methods* **5**, 135–146 (2008).
76. W. Kabsch, XDS. *Acta Crystallogr. D Biol. Crystallogr.* **66**, 125–132 (2010).
77. A. J. McCoy, R. W. Grosse-Kunstleve, P. D. Adams, M. D. Winn, L. C. Storoni, R. J. Read, Phaser crystallographic software. *J. Appl. Cryst.* **40**, 658–674 (2007).
78. G. N. Murshudov, P. Skubák, A. A. Lebedev, N. S. Pannu, R. A. Steiner, R. A. Nicholls, M. D. Winn, F. Long, A. A. Vagin, REFMAC5 for the refinement of macromolecular crystal structures. *Acta Crystallogr. D Biol. Crystallogr.* **67**, 355–367 (2011).
79. P. Emsley, K. Cowtan, Coot: Model-building tools for molecular graphics. *Acta Crystallogr. D Biol. Crystallogr.* **60**, 2126–2132 (2004).
80. G. N. Ramachandran, C. Ramakrishnan, V. Sasisekharan, Stereochemistry of polypeptide chain configurations. *J. Mol. Biol.* **7**, 95–99 (1963).
81. N. W. Moriarty, R. W. Grosse-Kunstleve, P. D. Adams, Electronic ligand builder and optimization workbench (eLBOW): A tool for ligand coordinate and restraint generation. *Acta Crystallogr. D Biol. Crystallogr.* **65**, 1074–1080 (2009).

Acknowledgments: We thank K. Kim for sharing PfPNP-related research materials for the purpose of this study, W. Phoo for valuable discussions about cocrystal structure analysis, and

Downloaded from http://stm.sciencemag.org/ by guest on February 8, 2019

all volunteers for providing blood for the parasite culture. **Funding:** This work was supported by NMRC MS-CETSA platform grant MOH/IAFCAT2/004/2015 to Z.B., P.N., A.L., and R.M.S.; Singapore Ministry of Education, Tier 2, MOE2015-T2-2-108 grant to Z.B.; Young Investigator Grant (YIG2015 A-STAR) to R.M.S.; Startup grant from NTU to P.N.; and grants from the Swedish Research Council and the Knut och Alice Wallenberg Foundation to P.N. **Author contributions**: P.N. and Z.B.: conceptualization; J.M.D.: manuscript preparation, CETSA, DSF, and enzymatic assays; H.Y.: CETSA and manuscript preparation; D.C.: protein cloning and expression, ITC, and crystallography; L.D.: mineCETSA; G.W.: drug synergy assays; A.L.: SPR; R.M.S.: MS experimental workflow design; N.P., Z.B., and P.N.: experimental design and manuscript revisions.
Competing interests: P.N. is the cofounder and a member of the board of directors of Pelago Bioscience AB and an inventor on a patent series originating from PTC/GB2012/050853 held by Pelago Bioscience AB that covers MS-CETSA. The other authors declare that they have no competing interests. **Data and materials availability:** All data relating to this study are present in the paper or Supplementary Materials.

Submitted 1 June 2018
Resubmitted 4 September 2018
Accepted 5 December 2018
Published 2 January 2019
10.1126/scitranslmed.aau3174

Citation: J. M. Dziekan, H. Yu, D. Chen, L. Dai, G. Wirjanata, A. Larsson, N. Prabhu, R. M. Sobota, Z. Bozdech, P. Nordlund, Identifying purine nucleoside phosphorylase as the target of quinine using cellular thermal shift assay. *Sci. Transl. Med.* **11**, eaau3174 (2019).

Downloaded from http://stm.sciencemag.org/ by guest on February 8, 2019

Science Translational Medicine

Identifying purine nucleoside phosphorylase as the target of quinine using cellular thermal shift assay

Jerzy M. Dziekan, Han Yu, Dan Chen, Lingyun Dai, Grennady Wirjanata, Andreas Larsson, Nayana Prabhu, Radoslaw M. Sobota, Zbynek Bozdech and Pär Nordlund

Sci Transl Med **11**, eaau3174.
DOI: 10.1126/scitranslmed.aau3174

Defining drug targets in malaria

Different classes of malaria drugs have been used for decades, even though the mechanisms of action have never been elucidated. To identify antimalarial drug targets, Dziekan *et al.* developed a protocol combining mass spectrometry and cellular thermal shift assay. The assay uses parasite lysate and intact infected red blood cells and was able to positively identify two known drug targets. They then investigated targets for quinine and mefloquine, revealing purine nucleoside phosphorylase as the top hit. Their results not only identify the likely target of these common drugs but also showcase an assay that could be widely used in antimalarial drug research.

ARTICLE TOOLS http://stm.sciencemag.org/content/11/473/eaau3174

SUPPLEMENTARY MATERIALS http://stm.sciencemag.org/content/suppl/2018/12/21/11.473.eaau3174.DC1

RELATED CONTENT
http://stm.sciencemag.org/content/scitransmed/10/447/eaar3619.full
http://stm.sciencemag.org/content/scitransmed/9/397/eaaf9377.full
http://stm.sciencemag.org/content/scitransmed/9/387/eaad9735.full

REFERENCES This article cites 77 articles, 25 of which you can access for free
http://stm.sciencemag.org/content/11/473/eaau3174#BIBL

PERMISSIONS http://www.sciencemag.org/help/reprints-and-permissions

Use of this article is subject to the Terms of Service

Science Translational Medicine (ISSN 1946-6242) is published by the American Association for the Advancement of Science, 1200 New York Avenue NW, Washington, DC 20005. 2017 © The Authors, some rights reserved; exclusive licensee American Association for the Advancement of Science. No claim to original U.S. Government Works. The title *Science Translational Medicine* is a registered trademark of AAAS.

Downloaded from http://stm.sciencemag.org/ by guest on February 8, 2019